Pairing Instability in Helical Vortices

Hadrien Bolnot, Stéphane Le Dizès, and Thomas Leweke

1 Introduction

The stability properties of helical vortices are of interest for applications such as wind turbine and helicopter wakes. In the former, they contribute to the transition from an organised vortex system to a turbulent wake behind the rotor, and in the latter they may be related to the inception of the so-called Vortex Ring State of the wake of a helicopter in steep descent [2, 7]. In this work, we consider the particular instability that leads to vortex pairing, for which previous experimental [1, 4] and numerical [5] studies have shown that it plays an important role in rotor wakes. In the following, we recall a few theoretical results concerning this phenomenon, and then present experimental observations of pairing in a single helical vortex under carefully controlled conditions.

2 Pairing Instability of Vortex Arrays

Vortex pairing is a process occurring in (infinite) arrays of identical concentrated vortices, whereby small perturbations of their initially equidistant positions are amplified in a way that neighbouring vortices approach each other and group in pairs. It occurs, e.g., in shear layers, as a secondary instability of the Kelvin-Helmholtz instability. Pairing is distinct from merging of two vortex cores of like-signed vorticity into a single one, which occurs when the two initial vortices come sufficiently close to each other (see, e.g., [9]). Merging may take place during the late stages of the pairing instability in arrays of real (distributed) vortices.

Systems of helical vortices, such as those found in the wake of a rotor, present locally arrays of identical curved vortices, which are expected to exhibit the pairing

Hadrien Bolnot · Stéphane Le Dizès · Thomas Leweke
IRPHE UMR 7342, CNRS, Aix-Marseille Université, 13384 Marseille, France
e-mail: Thomas.Leweke@irphe.univ-mrs.fr

M. Hölling et al. (eds.), *Wind Energy – Impact of Turbulence,*
Research Topics in Wind Energy 2,
DOI: 10.1007/978-3-642-54696-9_4,

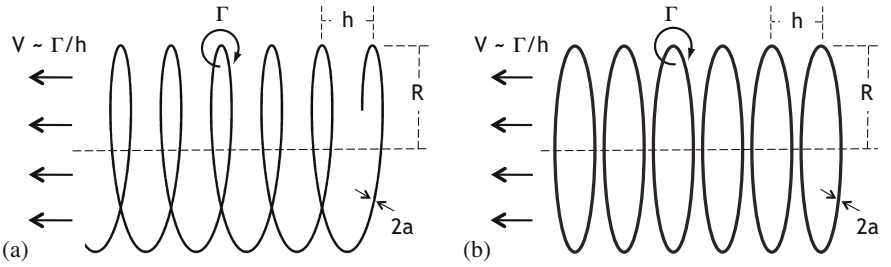

Fig. 1 Geometry and parameters of (a) a helical vortex filament and (b) an array of vortex rings

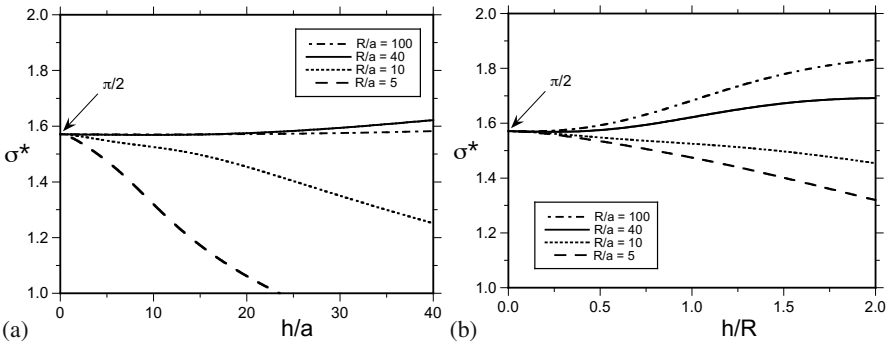

Fig. 2 Growth rate of the pairing instability for an array of vortex rings, as function of the separation h normalised by (a) the core size and (b) the helix radius (after [8])

instability. The simplest system consists in a single helical vortex filament, characterised by its circulation Γ and core radius a, as well as the helix radius R and pitch h (Fig. 1a). In the frame of reference where the fluid at infinity has no velocity in the direction of the helix axis, the fluid inside the helix moves at a speed of the order of Γ/h, and the helix itself moves with a velocity of roughly half this value ($\Gamma/2h$). The latter velocity and h are used here for non-dimensionalisation.

For small pitch ($h \ll R$), the helix geometry is locally very similar to that of an array of axisymmetric vortex rings (Fig. 1b). Levy & Forsdyke [8] have treated analytically the stability of such a system with respect to pairing of neighbouring vortex rings. Figure 2 shows the non-dimensional growth rate $\sigma^* = \sigma \cdot (2h^2/\Gamma)$ of the pairing instability as function of the geometric parameters. These were calculated using the same procedure as in [8], including also the effects of a smooth (Gaussian) vorticity distribution and of an axial core flow (see Sect. 3, Fig. 4b), as well as the variation of core size through stretching. For small separation/pitch ($h \ll R$) and small core size ($a \ll R$), which includes most configurations relevant for applications, the growth rate approaches the value $\pi/2$, i.e., the growth rate of the pairing instability for a single [3] or double [6] row of point vortices in two dimensions.

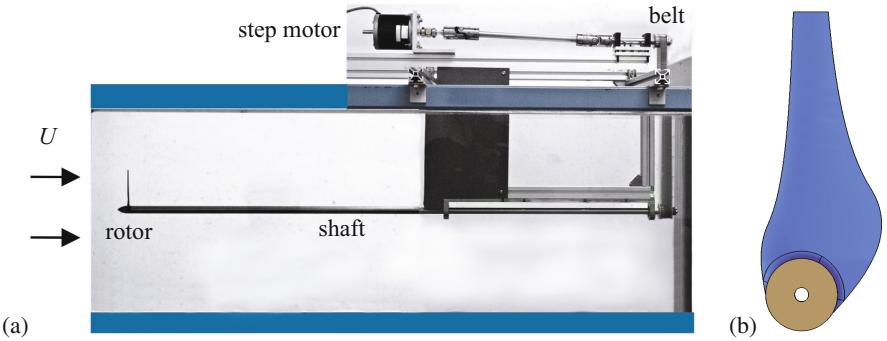

Fig. 3 (a) Side view of the water channel test section, showing the set-up used to generate a single helical vortex. (b) Plan view of the blade geometry.

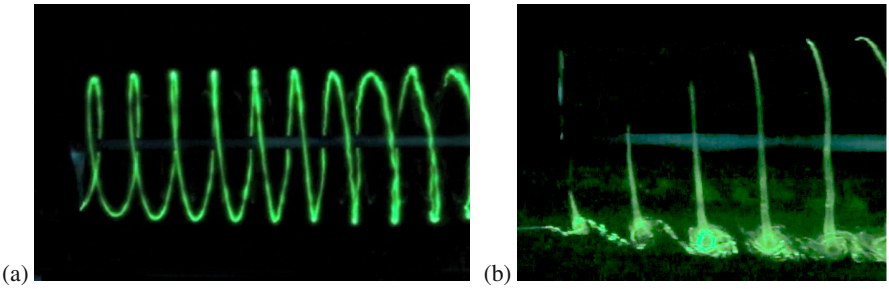

Fig. 4 Dye visualisation of the unperturbed helical vortex with $h/R = 0.53$ at $Re_\Gamma = 11500$. (a) Dye washed off the blade tip; (b) dye injected at a fixed position near the edge of the rotor disk.

3 Experiments

Experiments on the controlled pairing of a single helical vortex were carried out in a recirculating free-surface water channel with a test section of dimensions 38 cm (width) $\times$ 50 cm (height) $\times$ 150 cm (length). The vortex was generated near the test section entry by a single-bladed rotor mounted on a shaft and driven by a computer-controlled stepper motor outside the test section using a belt (Fig. 3a). The rotor blade geometry (Fig. 3b) is based on the low-Reynolds number airfoil A18 by Selig *et al.* [11], with chord and twist distributions designed to operate in the wind turbine regime and produce a constant radial circulation distribution (Joukowsky rotor, see e.g. [10]) over the outer 75% of the span, in order to generate a highly concentrated tip vortex. The rotor has a radius $R_o = 80$ mm and a tip chord $c = 10$ mm. For the present set of experiments, it is rotated at a frequency $f = 6$ Hz and placed in a uniform flow with a free stream velocity $U = 36$ cm/s, resulting in a tip speed ratio $\lambda = 8.4$. The tip chord Reynolds number is $Re_c = 2\pi R_o f c/\nu = 30000$, and the one based on the vortex circulation Γ (determined from Particle Image Velocity measurements) is $Re_\Gamma = \Gamma/\nu = 11500$. ν is the kinematic viscosity.

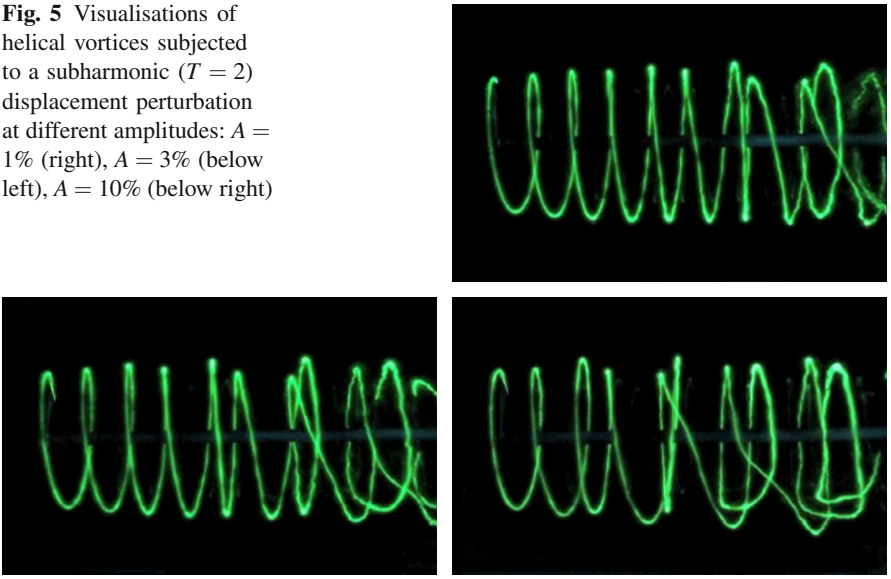

Fig. 5 Visualisations of helical vortices subjected to a subharmonic ($T = 2$) displacement perturbation at different amplitudes: $A =$ 1% (right), $A = 3\%$ (below left), $A = 10\%$ (below right)

The helical vortex structure is visualised using fluorescent dye (fluorescein) washed off the blade tip and illuminated by the light of an argon ion laser. Figure 4 shows the vortex produced for the present set of conditions, it is regular and unperturbed for about 10 helix turns. Dye injection at a fixed location near the blade tip trajectory (Fig. 4b) reveals the presence of a strong flow inside the core along the vortex axis. The dye pattern visualises the corresponding axial velocity profile and allows an estimate of the peak velocity V_a and the vortex core diameter $2a$ (width of the profile at $1/e$ of its maximum). The helix parameters are here found as: $h/R = 0.53$, $h/a = 20$, $R/a = 38$, $V_a = 0.4(\Gamma/2\pi a)$.

Pairing of successive helix loops was then induced by a controlled perturbation of the blade rotation, resulting in a varying streamwise displacement of the vortex. The modified helix geometry can be expressed as:

$$z/h = \theta/2\pi + A\cos(\theta/T), \tag{1}$$

where z and θ are the downstream and azimuthal positions, and A the relative displacement amplitude. For $T = 2$, successive helix loops are displaced in opposite directions, with an amplitude varying in the azimuthal direction, triggering local pairing. Figure 5 shows the vortex structure for three different amplitudes of forcing, with the maximum displacement occurring at the top (the perturbation vanishes at the bottom). A displacement of as little as 1% of h is seen to trigger the pairing instability, leading to a grouping and 'swapping' of successive loops as the helix moves downstream. The azimuthal variation of the pairing results in a complicated three-dimensional vortex structure, but no merging or breakdown to small-scale structures is seen. As the amplitude is increased, the deformations appear closer to the rotor, as expected.

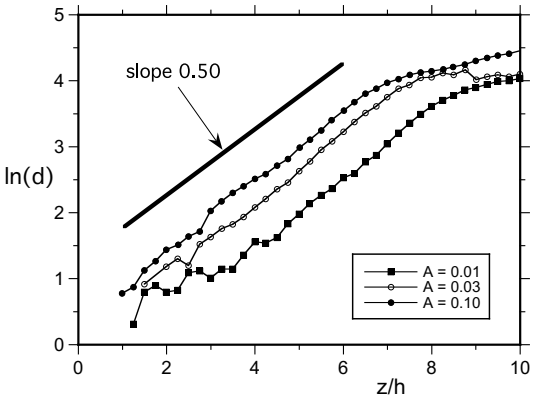

Fig. 6 Measurements of the amplitude d (in arbitrary units) of the pairing perturbation as function of downstream distance from visualisation sequences of the cases shown in Fig. 5

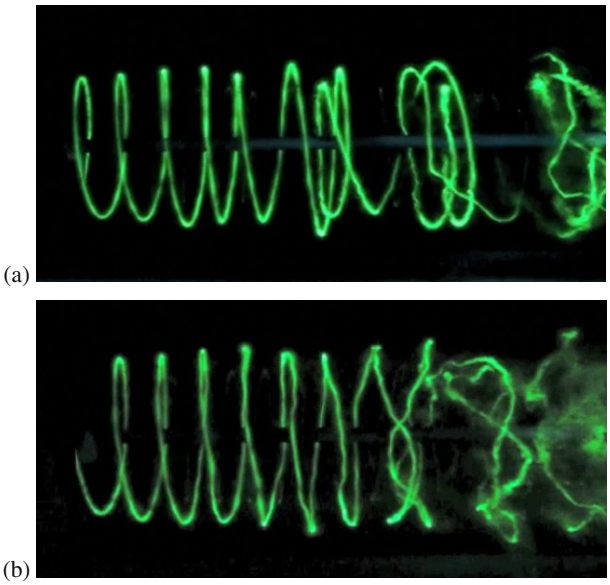

Fig. 7 Examples of more general displacement perturbations leading to instability. (b) Tripling ($T = 3$ and $A = 3\%$); (b) Short-wave perturbation ($T = 1/4$, $A = 10\%$).

The growth rate of the pairing instability can be estimated from the evolution of the displacement d of the vortex, with respect to the unperturbed position, which can be measured from video sequences of visualisations such as in Fig. 5. The result for these three cases is plotted in Fig. 6; the spatial growth rate σ_s is found to be close to $0.5/h$. Using the (measured) convection velocity V_c of the helix, one can obtain an estimate of the temporal growth rate $\sigma = \sigma_s V_c$, leading finally to a non-dimensional growth rate $\sigma^* = 1.2$ for these experiments. This is about 25% lower than the theoretical prediction ($\sigma^* \approx \pi/2$) for a row of vortex rings with the same geometrical parameters (Fig. 2). The difference may be due to the non-uniform nature of the

pairing for a single helix. The effect of the central hub vortex, always present in the wake of a rotor, also needs to be clarified. Further experiments involving two helical vortices (two-bladed rotor), where pairing can occur globally, are underway.

Vortex perturbations of the form given in Eq. (1) can be used to trigger various other types of 'pairing'. Two examples are shown in Fig. 7: a perturbation of period $T = 3$, leading to a grouping of three successive helix loops, and a perturbation on a shorter length scale ($T = 1/4$, four wavelengths in one turn). The latter case is seen to exhibit a breakdown of the vortex structure, triggered by local pairing and merging. It bears striking similarities with the numerical simulation results obtained by Ivanell *et al.* [5].

4 Conclusion

The experimental observation of the dynamics of a single helical vortex under carefully controlled conditions has shown that this flow is highly receptive to a variety of displacement perturbations leading to pairing of successive helix loops or more complicated three-dimensional deformations involving local merging and breakdown. These findings are coherent with the results from previous experimental studies of rotor wakes (e.g., [1, 4]), where helix loop grouping is consistently observed in a way which reflects the symmetry of the set-up (pairing for two blades, tripling for three blades, etc.), suggesting that this phenomenon might be triggered by small asymmetries in the rotor geometry. The great sensitivity of the rotor wake to displacement perturbations, and the fact that their amplitude influences the distance over which the helical wake evolves, may add further insight into the effect of rotor vibrations or external turbulence on the development of wind turbine wakes, and potentially lead to ideas for their control.

Acknowledgement. This work is supported by EUROCOPTER S.A.S., under contract no. IPEC 0187N/2009.

References

1. Alfredsson, P.H., Dahlberg, J.-Å.: Technical Note AU-1499 (Part 7), The Aeronautical Research Institute of Sweden, Stockholm (1979)
2. Bolnot, H., Le Dizès, S., Leweke, T.: AIAA Paper 2011-3927 (2011)
3. Branger, P., Chomaz, J.M.: Phys. Rev. Lett. 78, 658 (1997)
4. Felli, M., Camussi, R., Di Felice, F.: J. Fluid Mech. 682, 5 (2011)
5. Ivanell, S., Mikkelsen, R., Sørensen, J.N., Henningson, D.: Wind Energy 13, 705 (2010)
6. Lamb, H.: Hydrodynamics, 6th edn. Cambridge University Press (1932)
7. Leishman, J.G., Bhagwat, M.J., Ananthan, S.: J. Am. Helicopter Soc. 49, 160 (2004)
8. Levy, H., Forsdyke, A.G.: Proc. R. Soc. Lond. A 114, 594 (1927)
9. Meunier, P., Le Dizès, S., Leweke, T.: C. R. Physique 6, 431 (2005)
10. Okulov, V.L., Sørensen, J.N.: J. Fluid Mech. 649, 497 (2010)
11. Selig, M.S., Guglielmo, J.J., Broeren, A.P., Giguere, P.: Summary of Low-Speed Airfoil Data, SoarTech, Virginia Beach, vol. 1 (1995)